



Published in final edited form as:

Wound Repair Regen. 2020 July ; 28(4): 470–479. doi:10.1111/wrr.12812.

Sex Differences in Murine Myocutaneous Flap Revascularization

Jacquelyn S. Brandenburg, DO¹, Ross M. Clark, MD¹, Brittany Coffman, MD², Geetanjali Sharma, PhD³, Helen J. Hathaway, PhD⁴, Eric R. Prossnitz, PhD³, Thomas R. Howdieshell, MD¹

¹Department of Surgery, University of New Mexico Health Sciences Center, Albuquerque, New Mexico

²Department of Pathology, University of New Mexico Health Sciences Center, Albuquerque, New Mexico

³Department of Internal Medicine, University of New Mexico Health Sciences Center, Albuquerque, New Mexico

⁴Department of Cell Biology and Physiology, University of New Mexico Health Sciences Center, Albuquerque, New Mexico

Abstract

Sex differences in susceptibility to ischemia/reperfusion injury have been documented in humans. Premenopausal women have a lower risk of ischemic heart disease than age-matched men, whereas after menopause, the risk is similar or even higher in women. However, little is known about the effects of sex on myocutaneous ischemia/reperfusion. To explore sex differences in wound revascularization, we utilized a murine myocutaneous flap model of graded ischemia. A cranial-based, peninsular-shaped, myocutaneous flap was surgically created on the dorsum of male and female mice. Physiological, pathological, immunohistochemical, and molecular parameters were analyzed. Flaps created on female mice were engrafted to the recipient site resulting in nearly complete viability at post-operative day 10. In contrast, distal full-thickness myocutaneous necrosis was evident at 10 days post-surgery in male mice. Over the 10 day study interval, laser speckle imaging documented functional revascularization in all flap regions in female mice, but minimal distal flap reperfusion in male mice. Day 10 immunostained histologic sections confirmed significant increases in distal flap vessel count and vascular surface area in female compared to male mice. RT-PCR demonstrated significant differences in growth factor and metabolic gene expression between female and male mice at day 10. In conclusion, in a graded-ischemia wound healing model, flap revascularization was more effective in female mice. The recognition and identification of sex-specific wound healing differences may lead to a better understanding of the underlying mechanisms of myocutaneous revascularization and drive novel

Correspondence: Thomas R. Howdieshell, MD, Department of Surgery, Trauma/Surgical Critical Care, MSC10-5610, University of New Mexico HSC, Albuquerque, NM 87131, Phone: 505- 272-6441, Fax: 505-272-0434, thowdieshell@salud.unm.edu; rhowdieshell@comcast.net.

Author Contributions: TRH, HJH, and ERP designed and interpreted experiments. JSB, RMC, BBC, GS, and TRH performed experiments and analyzed data. TRH wrote the manuscript. All authors reviewed and edited the manuscript.

Disclosures: None.

discovery to improve soft tissue wound healing following tissue transfer for traumatic injury and cancer resection.

Keywords

Ischemia/reperfusion; angiogenesis; myocutaneous flap

INTRODUCTION

Sex differences exist in almost every aspect of human physiology and disease. In virtually any physiological study, the frequent focus on a single sex threatens to limit the impact of research findings, as results may be relevant to only half of the population. To correct this bias, the National Institutes of Health has mandated researchers consider sex as a biological variable in preclinical research by including both sexes in research designs. The importance of studying male and female models is not just a matter of being inclusive. Rather, the comparison of the two sexes raises questions that would otherwise not be asked such as what are the mechanisms that provide greater protection in one sex versus the other, and can those mechanisms and factors be harnessed for better therapy in both sexes¹⁻³.

Sex disparities regarding pathogenic mechanisms, age of onset, progression, and therapy suitability are common in human disease⁴. Sex differences in ischemia-reperfusion injury have been investigated in animal models, and provided evidence for differences in responses to ischemia in the heart, brain, kidney, liver, and intestine. Beneficial effects of the female hormone estrogen and/or deleterious effects of the male hormone testosterone acting through their respective receptors are usually held responsible⁵⁻⁹.

Microsurgical free-tissue transfer has become a common practice in reconstructive surgery to provide an efficient approach to restore the form and function of complex tissue defects due to traumatic injury or cancer resections. The loss of skin, muscle, and even bone after avulsion or amputation injuries or after tumor resections in the head, neck, trunk, or extremities represent reconstructive challenges for surgeons. Microsurgical reconstructions with composite or single free-tissue transfers are ideal options to cover these three-dimensional defects. The incidence of complications following flap transfer necessitates a better understanding of the pathophysiological processes of ischemia-reperfusion¹⁰⁻¹¹. Even though the skin and skeletal muscle contain functional estrogen and androgen receptors and therefore are potential hormone-responsive organs, the impact of sex on the pathogenesis of myocutaneous flap ischemia-reperfusion remains unclear¹²⁻¹³.

Therefore, we explored sex differences in wound revascularization using a murine myocutaneous flap model of graded ischemia. Our results reveal that surgically created flaps in female mice engrafted to the recipient site with far greater viability and revascularization than in male mice. Male flaps displayed distal full-thickness myocutaneous necrosis. Significant differences in local growth factor and metabolic gene expression existed between sexes. These substantial sex-dependent differences in wound healing offer the possibility to improve healing in males, and through an understanding of the mechanisms involved, to improve healing in both sexes.

MATERIALS AND METHODS

Mouse myocutaneous flap model and wound morphology analysis.

All animals were treated humanely in accordance with the National Research Council's "Guide for the Care and Use of Laboratory Animals" as a part of a protocol approved by the University of New Mexico's animal review committee. Aged-matched female (10 ± 2 weeks of age) and male (10 ± 2 weeks of age) C57BL6 mice (Harlan Laboratories, Indianapolis, IN, USA) underwent anesthesia with isoflurane (1-3%) via nose cone inhalation. Post-operative analgesia was provided using a single subcutaneous dose (0.01 mg/kg) of buprenorphine hydrochloride. All mice were weighed pre-operatively and at day 10 using a precision scale (XP-600, Denver Instruments, Denver, CO, USA). A total of 30 mice were used in the study, ten male and 10 female mice underwent flap surgery, and 5 male and 5 female mice were sacrificed as nonoperative back tissue controls.

After maintenance of inhalation anesthesia, hair was removed from the mouse back skin using electric clippers, and the site was prepped with povidone-iodine and 70% ethanol. The mice underwent surgical creation of a peninsular flap (3 cm in length and 1.5 cm in width) consisting of skin, adipose tissue, and panniculus carnosus muscle by making 3 soft tissue incisions. Precision in flap dimensions was confirmed by laser template projection and measurement by caliper¹⁴. The flap was elevated cranially and re-approximated to the back skin with 6-0 monofilament sutures. After surgery, each animal was singly housed and received water and food ad libitum.

At 0 hours (immediately following flap surgery), 2, 5, and 10 days post-surgery, the dorsal flap was photographed for image analysis using a Nikon 070 digital camera (Nikon Instruments, Melville, NY, USA) which was equipped with a macro lens and mounted on a tripod at consistent height. The percentage of flap surface area was computed using a standard planimetry method. The percentage of visible flap necrosis was calculated by dividing the measured area necrosis by the flap surface area at each specific day. Flap area index was calculated by dividing the measured flap surface area at a specific day by the immediate post-operative flap area (control) to document the importance of skin and panniculus muscle necrosis on flap size¹⁴.

Laser speckle perfusion imaging.

At 0 hours, 2 days, 5 days, and 10 days after surgery, each animal underwent inhalation anesthesia in prone position, and laser speckle perfusion imaging was performed with the Full-Field Laser Perfusion Imager (FLPI, Moor Instruments, Essex, UK) in low-resolution/high-speed setting at a display rate of 25 Hz, time constant of 1.0 s, and camera exposure time of 20 ms. The instrument head containing the CCD (charged coupled device) camera was positioned 30 cm above the mouse back skin tissue surface using an articulating arm. Real-time data was acquired in the Live Image measurement mode. The contrast images were processed to produce a scaled color-coded Live Flux image (red, high perfusion; blue, low perfusion), which correlated with the blood flow velocity in the tissue.

The FLPI instrument reports perfusion in arbitrary units. To assign values to a measurement, the imager was calibrated using a reference flux signal generated by the laser light scattered

from a suspension of polystyrene microspheres in water undergoing thermal or Brownian motion. From kinetic theory, the average velocity of the microspheres is proportional to the square root of the temperature in Kelvin. All measurements were performed at a room temperature of 20° C¹⁵.

For each time point examined, 10 single-frame images acquired at end expiration (no torso movement) were analyzed in the repeat image measurement window utilizing 3 identical regions of interest (ROI): cranial, central, and caudal. At each time point, the mean perfusion in each ROI was calculated for control skin and the peninsular flaps¹⁶.

Tissue harvest, histology, and immunochemical staining.

Mice, either without surgery (utilized as tissue controls) or 10 days following flap surgery, were humanely sacrificed by CO₂ inhalation for histologic and molecular examination. Unoperated back skin (controls) or day 10 flap was excised using sterile technique and transversely bisected yielding a proximal and distal tissue specimen. Histology and isolated RNA were processed in two flap regions (proximal and distal) rather than three ROIs due to sample volume requirements. One half of the tissue was fixed in IHC Zinc Fixative (BD Biosciences-Pharmingen, San Diego, CA, USA) for 24 hours, processed, and paraffin embedded. Serial sections (4 µm) were dewaxed in xylene, gradually hydrated through graded ethanol and finally phosphate-buffered saline solution, before staining with Hematoxylin and Eosin (Vector Laboratories, Burlingame, CA, USA) or CD-31 immunohistochemistry for the determination of panniculus muscle viability and microvascular density respectively. The remaining half of the excised flap was immersed in 500 µL of RNAlater RNA Stabilization Reagent (Qiagen, Valencia, CA, USA) and stored at 4°C for later RNA isolation and purification.

Blood vessel identity was determined by CD-31 immunostaining. After dewaxing and hydration, sections were incubated for 10 minutes in 3% hydrogen peroxide in methanol to block endogenous peroxidase activity, washed in phosphate-buffered saline, and incubated with primary antibody (rat anti-mouse CD-31, 1:50, BD Biosciences-Pharmingen) for 1 hour at room temperature in a humidified chamber. Next, the sections were incubated with a biotinylated secondary antibody (anti-rat immunoglobulin horseradish peroxidase kit, 1:50, BD Biosciences-Pharmingen) for 30 minutes at room temperature. The streptavidin-horseradish peroxidase reagent was applied for 30 minutes followed by 3,3'-diaminobenzidine (DAB) chromogen for 5 minutes. The sections were counterstained with Vector Hematoxylin QS (Vector Laboratories) with quick immersion. The DAB substrate-chromogen resulted in a brown-colored precipitate at the antigen site.

Panniculus muscle viability and microvascular density determination.

Multiple full- thickness male and female nonoperative control tissue sections and day 10 male and female flap biopsy sections (3 proximal and 3 distal sections per mouse) were analyzed with mean values reported. A Zeiss microscope with attached digital camera (Carl Zeiss Microimaging, Jena, Germany) was used for image acquisition. The magnified image (X100) of the slide section was analyzed with SlideBook image analysis software (SlideBook 5.0, Intelligent Imaging Innovations, Santa Monica, CA, USA). The muscle area

index was determined with image analysis of Hematoxylin and Eosin stained sections by dividing the viable panniculus carnosus muscle surface area at day 10 by the unoperated flap muscle area. Skin, subcutaneous tissue, and panniculus muscle vessel counts and vascular luminal cross-sectional surface areas were determined with image analysis of CD-31 immunostained sections^{14, 16}.

RNA isolation and purity.

Tissue samples were homogenized using a rotor-stator (VWR Pellet Mixer, VWR, West Chester, PA, USA) and QiaShredder (Qiagen) biopolymer shredding system according to the manufacturers' instructions. RNA concentration was determined by the absorbance at 260 nm in a spectrophotometer (NanoDrop 2000, Thermo Fisher Scientific, Waltham, MA, USA). RNA purity was confirmed by a spectrophotometric ratio (A_{260}/A_{280}) of 1.9-2.1, and by sharp bands for 28S and 18S ribosomal RNA on agarose gel electrophoresis¹⁶.

Gene expression.

TaqMan gene expression analysis consisted of a specific pair of unlabeled polymerase chain reaction (PCR) primers and a TaqMan probe (Applied Biosystems, Foster City, CA, USA) with glyceraldehyde-3-phosphate dehydrogenase utilized as an endogenous housekeeping control. The TaqMan gene expression analysis was performed using the following probe/primers: VEGFa (vascular endothelial growth factor a, Mm 00437306_m1), FGF2 (fibroblast growth factor 2, Mm 01285715_m1), Notch1 (Mm 00627185_m1), PFKFB3 (6-phosphofructo-2-kinase/fructose-2,6-biphosphatase 3, Mm 00504650_m1), CPT1a (carnitine palmitoyltransferase 1a, Mm01231183_m1), HX2 (hexokinase 2, Mm00443385_m1), KLF2 (kruppel-like factor 2, Mm00500486_g1), FOXO1 (forkhead box protein O1, Mm 00490671_m1), and GAPDH (glyceraldehyde-3-phosphate dehydrogenase, Mm 999999_g1). Real-time TaqMan PCR assays were performed on the Applied Biosystems Viia 7 Real-Time PCR System. Male and female nonoperative control and day 10 male and female flap myocutaneous tissue RNA samples were run in triplicate on 96-well plates with one gene of interest per plate. Changes in expression of a particular gene between control and day 10 interval was quantitated by comparing the difference in cycle threshold (C_t) values (C_t) after normalization. Values for controls and day 10 time intervals were used in the calculation of fold change only if their C_t value was < 35 confirming expression.

Statistical analysis.

All data are expressed as mean \pm standard error of the mean (SEM). Statistical analysis was performed with SPSS 15.0 software (SPSS Inc., Chicago, IL, USA). Differences among groups and between baseline and subsequent time points were determined with Student's t test or repeated-measures analysis of variance with Tukey significant difference test used for post hoc analysis. All calculations and statistical analysis of the PCR data was performed using QuantStudio V1.3 Real-Time PCR software (Applied Biosystems). Statistical significance was accepted at a p value < 0.05 .

RESULTS

Body weights and control skin morphology.

Despite age-matching, significant differences in pre-operative body weights and control skin dimensions were evident between sexes. The mean pre-operative weight of female mice was 19.6 ± 1.8 grams (range 18.2-20.1 grams) compared to male mean weight of 25.2 ± 1.8 grams (range 24.6-26.8 grams) ($p < 0.05$). There was no significant change in weight over the 10 day study period in either sex (Figure 1A). Control skin thickness and proportions of skin layers varied significantly between sexes. The major difference was the dermal thickness in male mice (mean 395 ± 15 μm , range 380-405 μm) was much greater than in female mice (mean 100 ± 10 μm , range 88-109 μm), resulting in a 23% greater total skin thickness in male (mean 585 ± 15 μm , range 579-600 μm) compared to female mice (mean 410 ± 12 μm , range 392-419 μm) ($p < 0.05$). The hypodermis or subcutaneous fat layer was significantly thicker in female mice (female: mean 215 ± 8 μm , range 209-220 μm ; male: mean 55 ± 5 μm , range 50-60 μm) ($p < 0.05$). There was no thickness difference in epidermis (female: mean 10 ± 2 μm , range 8-11 μm ; male: mean 9 ± 2 μm , range 8-10 μm) or panniculus muscle (female: mean 80 ± 6 μm , range 76-84 μm ; male: mean 85 ± 9 μm , range 80-91 μm) noted between sexes (Figures 1B, C, D).

Myocutaneous flap viability and histopathology.

Persistent distal ischemia presenting as superficial blisters (epidermolysis) was observed in male distal flaps beginning on day 2. By day 10, male flaps were reduced in size due to lack of flap engraftment to the recipient site (paraspinal musculature), distal flap full-thickness necrosis, and resultant flap contraction. In contrast, female myocutaneous flaps engrafted to the recipient bed with negligible contraction and nearly complete skin and muscle viability (Figures 2A, B). Quantitative image analysis revealed that visible cutaneous necrosis in male flaps accounted for a mean of $30.8 \pm 5.7\%$ (range 25.6-37.0%) of the total flap surface area at its maximum on post-operative day 10, whereas in female mice, visible necrosis represented only a mean of $5.7 \pm 0.9\%$ (range 4.0-6.1%) of total flap area at the same time interval ($p < 0.001$). In addition, planimetry documented a significant reduction in flap surface area at day 10 in male compared to female mice (flap area index: male, mean $60 \pm 8\%$, range 54-63%; versus female, mean $88 \pm 7\%$, range 80-94%, $p < 0.05$) (Figures 2C, D).

Histopathology revealed that the contraction in the size of male flaps occurred as a consequence of distal flap cutaneous and panniculus carnosus muscle necrosis (day 10 muscle area index: female, mean $92 \pm 5\%$, range 88-97%; male, mean $35 \pm 4\%$, range 32-40%), and proliferation of the surrounding back skin epidermis producing elevation of the distal flap eschar and resultant epithelial closure of the residual wound by secondary healing. Minimal contraction was evident in female flaps due to viable distal skin and panniculus muscle, and complete flap engraftment to the recipient bed (Figures 2E, F, G).

Perfusion imaging.

Creation of the cranial-based, peninsular-shaped, myocutaneous flap by 2 longitudinal incisions and connecting transverse caudal incision provided a reproducible gradient of ischemia in male and female mice from interruption of the segmental and underlying blood

supply (16). Before operative intervention (preop), mouse back skin perfusion was comparable across cranial, central, and caudal ROIs in both sexes (female pre-operative total flap perfusion 170 ± 19 PU versus male pre-operative total flap perfusion 182 ± 12 PU).

Immediately after flap creation (POD 0), flap perfusion declined in a nearly identical cranial to caudal gradient in both groups. However, over the 10 day study period, in female mice, laser imaging documented markedly increased perfusion in each ROI at all time points compared to immediate post-operative values. By day 10, in female flaps, cranial, central, and caudal ROI perfusion actually surpassed pre-operative or baseline values, an indication of effective flap revascularization (Figure 3).

In contrast, in male mice, cranial ROI perfusion peaked at day 2 at a value comparable to female day 2 cranial ROI perfusion, and subsequently declined toward baseline by day 10. In distinction to female flaps, male central and caudal ROI perfusion peaked at day 2 at values at or below baseline perfusion, with limited change over the remaining study period. At day 10, male caudal ROI perfusion was less than baseline perfusion, suggesting lack of distal flap revascularization (Figure 3).

Microvascular anatomy and quantitation.

To investigate the quantity and quality of the microvasculature responsible for the spatiotemporal change in flap perfusion, CD-31 immunostaining and digital image analysis of proximal and distal histologic specimens were utilized to determine vessel count and vascular luminal surface area. Control vessel counts (female, mean $47 \pm 10/\text{mm}^2$, range $41\text{-}52/\text{mm}^2$; male, mean $49 \pm 8/\text{mm}^2$, range $42\text{-}51/\text{mm}^2$) and surface area estimates (female, mean $2,550 \pm 145 \mu^2/\text{mm}^2$, range $2,390\text{-}2,640 \mu^2/\text{mm}^2$; male, mean $2,610 \pm 130 \mu^2/\text{mm}^2$, range $2,510\text{-}2,695 \mu^2/\text{mm}^2$) were comparable in female and male mice. By day 10, in female mice, there was a significant increase in distal flap vessel number (mean $125 \pm 11/\text{mm}^2$, range $118\text{-}130/\text{mm}^2$) ($p < 0.001$), and proximal (mean $15,100 \pm 185 \mu^2/\text{mm}^2$, range $14,010\text{-}16,850 \mu^2/\text{mm}^2$) ($p < 0.001$) and distal (mean $7,500 \pm 145 \mu^2/\text{mm}^2$, range $7,000\text{-}8,010 \mu^2/\text{mm}^2$) ($p < 0.01$) vascular surface area compared to female control back tissue. In contrast, in male mice at day 10, there was no increase in distal flap vessel number (mean $44 \pm 7/\text{mm}^2$, range $40\text{-}51/\text{mm}^2$) or surface area (mean $2,250 \pm 125 \mu^2/\text{mm}^2$, range $2,000\text{-}2,650 \mu^2/\text{mm}^2$) compared to male control back tissue. However, there was an increase in male proximal flap surface area at day 10 (mean $10,000 \pm 160 \mu^2/\text{mm}^2$, range $9,900\text{-}11,050 \mu^2/\text{mm}^2$) compared to male control back tissue ($p < 0.01$) (Figures 4A, B).

Quantification and localization of the microvasculature corroborated the changes in flap perfusion demonstrated by laser speckle contrast imaging. Dilatation of existing cranial and central region (proximal) vessels and new vessel growth or neovascularization from the recipient paraspinal muscle vasculature into the distal flap were responsible for flap revascularization and viability in female mice. Conversely, in male mice, there was dilatation of proximal flap vasculature but no significant distal neovascularization resulting in distal flap myocutaneous necrosis (Figures 4C, D).

Gene expression.

Recent research indicates that endothelial cells can only execute the orders of growth factors if they accordingly adapt their metabolism, suggesting that endothelial cell metabolism could regulate angiogenesis^{17, 18}. Therefore, we examined female and male flaps for the expression of growth factor and metabolic genes known to be important in angiogenesis. Prior to flap creation (control), there was no significant difference in the myocutaneous tissue expression of any of the 8 study genes between female and male mice. However, at day 10, significant increases in the expression of FGF2 (mean fold increase 3.17 ± 0.25 , range 2.9-3.8, $p < 0.05$) and Notch1 (mean fold increase 2.55 ± 0.15 , range 2.4-2.8, $p < 0.05$) genes were evident in female compared to male flaps. Significant increases in the expression of CPT1a (mean fold increase 3.05 ± 0.2 , range 2.9-3.6, $p < 0.05$) and KLF2 (mean fold increase 3.81 ± 0.3 , range 3.2-4.2, $p < 0.05$) genes were documented in male compared to female flaps at day 10. There were no significant differences in VEGFa, PFKFB3, HX2, and FOXO1 expression noted between sexes (Figure 5).

DISCUSSION

Preclinical research has been biased with respect to sex. There has been a tendency to treat the sexes as equivalent, without consideration of how differences in the number and type of sex chromosomes and fluctuations of gonadal hormones impact experimental outcomes, thereby limiting understanding of the mechanisms that drive sexual dimorphism^{19, 20}. The NIH has recently recognized this gap in scientific knowledge and now mandates that studies be conducted in both sexes¹. Recent research provides novel evidence that visceral adipose tissue of female mice possesses greater levels of pro-angiogenic factors and vascularity than males in response to a high fat diet, and collagen metabolism is impaired in the colonic anastomosis of male compared with female rats during early wound healing^{21, 22}.

In gonadally intact rodents, it has been suggested that males should be compared to females on specific days of their 4 day estrous cycle to generate reliable data²³. However, a meta-analysis comparison of male and female rodents, with no regard to the stage of the estrous cycle, established that variability in most traits was equivalent in females and males, and that for most end points, it was unnecessary to stage the estrous cycle^{24,25}. Furthermore, female rodents frequently synchronize their estrous cycles as a result of chemosignals from pheromones if housed together^{26,27}.

Therefore, we investigated sex differences in myocutaneous wound revascularization using a murine model of graded flap ischemia in age-matched, gonadally intact, female and male mice. At initiation of the study, female mice weighed approximately 20% less than male mice. Our results reveal that significant pre-operative differences (nonoperative controls) were also evident in back skin thickness and morphology between the sexes. Female mouse skin was thinner with reduced dermal and increased subcutaneous fat composition compared to male mouse skin. Interestingly, control myocutaneous microvascular density was comparable between the sexes as was subcutaneous panniculus carnosus muscle thickness and histologic appearance. Laser speckle imaging demonstrated comparable baseline perfusion and a nearly identical graded-ischemic response to flap creation in female and male mice. However, functional revascularization of the distal flap, the region of greatest

ischemia, was significantly more effective in female mice. Planimetry confirmed greater flap surface area viability and reduced contraction in female compared to male mice. Histologic findings corroborating these visible features included healthy epidermis, dermis, and panniculus muscle with active angiogenesis and marked neovascularization of female distal flaps compared to full-thickness myocutaneous necrosis and lack of vascular ingrowth in male flaps.

Endothelial cells display a remarkable behavioral plasticity. Although quiescent for years, following an ischemic stimulus, endothelial cells can switch to an activated, highly proliferative, and migratory state in response to growth factor stimuli, primarily through VEGF and FGF signaling^{28,29}. Recent papers on glycolysis and fatty acid oxidation in endothelium reveal that metabolism drives vessel sprouting in parallel to well-established growth factor-based (genetic) signaling^{30,31}. However, little is known about the effects of sex on myocutaneous endothelial behavior.

Therefore, we assessed control and day 10 female and male flap tissue for the expression of a panel of growth factor and metabolic genes known to be important in angiogenesis. These included genes that direct endothelial proliferation, migration, and differentiation (VEGF α , FGF2, Notch1), control glycolytic metabolism (PFKFB3, HX2), regulate fatty acid oxidation (CPT1a), and modulate cellular quiescence (KLF2, FOXO1)³²⁻³⁵. There was no difference in tissue gene expression between the sexes prior to flap creation. However, at day 10, significant increases in FGF2 and Notch1 gene expression were evident in female compared to male flaps. Conversely, significant increases in CPT1a and KLF2 gene expression were documented in male compared to female flaps at day 10. Finally, there were no significant differences in VEGF α , PFKFB3, HX2, and FOXO1 expression noted between the sexes. Whether these preliminary (control, day 10) molecular results represent effective, resolving neovascularization and maturation of microvasculature in female flaps, and inefficient revascularization with a persistent distal ischemic stimulus and sustained fatty acid oxidation in male flaps is unclear.

Physiological sex differences are largely driven by the hormones estrogen and testosterone and their respective receptors^{36,37}. The endogenous estrogen 17 β -estradiol (E2) is a key factor in promoting endothelial healing and angiogenesis. Proangiogenic signals including VEGF, FGF, and others have been shown to converge in endothelial cell metabolism^{38,39}. The often-beneficial effects of estrogen are mediated by both the nuclear estrogen receptors ER α and ER β , and the 7-transmembrane G protein-coupled estrogen receptor GPER^{40,41}. Whereas ER α and ER β have traditionally been recognized for their ligand induced transcriptional regulation, GPER has been shown to mediate many of the rapid signaling events of estrogen^{42,43}. The availability of GPER-selective ligands as well as knockout mice has contributed to understanding the role of GPER in many areas of physiology and disease pointing to possible therapeutic applications⁴⁴⁻⁴⁶. A recent report demonstrated E2-induced angiogenesis was mediated in part by GPER and required upregulation of the glycolytic activator PFKFB3⁴⁷. This finding unraveled a previously unrecognized mechanism of estrogen-dependent endocrine-metabolic crosstalk in endothelial biology. In future research utilizing this model, we plan to determine if nongenomic estrogen signaling via GPER plays an important role in the sex-dependent differences observed in this study.

In conclusion, in a graded-ischemia wound healing model, marked differences in flap surface area survival, local angiogenesis, and functional revascularization were evident between age-matched female and male mice. Recognition and identification of sex-specific wound healing differences may drive novel discovery to improve wound healing in both sexes.

Acknowledgments:

We thank Susan Tigert, research technician of the University of New Mexico Clinical and Translational Science Center (ULI TR001449) T-laboratory for technical assistance.

Sources of Funding: The authors were supported by University of New Mexico Department of Surgery grant (TRH), Center of Biomedical Research Excellence in Autophagy, Inflammation, and Metabolism (P20 GM121176), UNM Comprehensive Cancer Center (P30 CA118100), and NIH RO1 grants (CA 163890 and CA 194496, ERP).

REFERENCES

1. Clayton JA, Collins FS. Policy: NIH to balance sex in cell and animal studies. *Nature* 2014; 509:282–283. [PubMed: 24834516]
2. Tannenbaum C, Schwartz JM, Clayton JA, deVries GJ, Sullivan C. Evaluating sex as a biological variable in preclinical research: the devil in details. *Biol Sex Diff.* 2016; 7:13.
3. Danska JS. Sex matters for mechanism. *Sci Transl Med.* 2014; 6:258–265.
4. Lista P, Straface E, Brunelleschi S, Franconi F, Malorni W. On the role of autophagy in human diseases: a gender perspective. *J Cell Mol Med.* 2011; 15:1443–1457. [PubMed: 21362130]
5. Chen C, Hu LX, Dong T, Wang GQ, Wang LH, Zhou XP, Jiang Y, Murao K, Lu SQ, Chen JW, Zhang GX. Apoptosis and autophagy contribute to gender difference in cardiac ischemia-reperfusion induced injury in rats. *Life Sci.* 2013; 93:265–270. [PubMed: 23827240]
6. Zuo W, Zhang W, Chen NH. Sexual dimorphism in cerebral ischemia injury. *Eur J Pharmacol.* 2013; 711:73–79. [PubMed: 23652162]
7. Rodriguez F, Nieto-Ceron S, Fenoy FJ, Lopez B, Hernandez I, Martinez RR, Soriano MJ, Salom MG. Sex differences in nitrosative stress during renal ischemia. *Am J Physiol Regul Integr Comp Physiol.* 2010; 299:R1387–R1395. [PubMed: 20702799]
8. Crockett ET, Spielman W, Dowlatshahi S, He J. Sex differences in inflammatory cytokine production in hepatic ischemia-reperfusion. *J Inflamm (Lond).* 2006; 3:16–22. [PubMed: 17177998]
9. Szabo A, Vollmar B, Boros M, Menger MD. Gender differences in ischemia-reperfusion-induced microcirculatory and epithelial dysfunction in small intestine. *Life Sci* 2006; 78:3058–3065. [PubMed: 16413039]
10. Bui DT, Cordeiro PG, Hu QY, Disa JJ, Pusic A. Free flap reexploration: indications, treatment, and outcomes in 1193 free flaps. *Plastic and Reconstructive Surgery* 2007; 119:2092–2100. [PubMed: 17519706]
11. Vega S, Smartt JM Jr, Jiang S, Selber JC, Brooks CJ, Herrera HR, Serletti JM. 500 consecutive patients with free TRAM flap breast reconstruction: a single surgeon's experience. *Plastic and Reconstructive Surgery* 2008; 122:329–339. [PubMed: 18626347]
12. Kanda N, Watanabe S. Regulatory roles of sex hormones in cutaneous biology and immunology. *J Dermatol Sci.* 2005; 38:1–7. [PubMed: 15795118]
13. Zouboulis CC, Chen WC, Thornton MJ, Qin K, Rosenfield R. Sexual hormones in human skin. *Horm Metab Res.* 2007; 39:85–95. [PubMed: 17326004]
14. Clark RM, Coffman B, McGuire PG, Howdieshell TR. Myocutaneous revascularization following graded ischemia in lean and obese mice. *Diabetes, Metabolic Syndrome and Obesity: Targets and Therapy* 2016; 9:325–336.
15. Leahy MJ, Enfield JG, Clancy NT. Biphotonic methods in microcirculation imaging. *Medical Laser Application* 2007; 22:105–129.

16. McGuire PG, Howdieshell TR. The importance of engraftment in flap revascularization: confirmation by laser speckle perfusion imaging. *J Surg Res.* 2010; 164:e201–e212. [PubMed: 20863524]
17. Rohlenova K, Veys K, Miranda-Santos I, DeBock K, Carmeliet P. Endothelial cell metabolism in health and disease. *Trends in Cell Biology* 2018; 28(3):224–236. [PubMed: 29153487]
18. Draouli N, deZeeuw P, Carmeliet P. Angiogenesis revisited from a metabolic perspective: role and therapeutic implications of endothelial cell metabolism. *Open Biology* 2017; 7:1–8.
19. Miller VM, Reckelhoff JF, Sieck GC. Physiology's impact: stop ignoring the obvious-sex matters! *Physiology* 2014; 29:4–5. [PubMed: 24382865]
20. Morselli E, Frank AP, Santos RS, Fatima LA, Palmer BF, Clegg DJ. Sex and gender: critical variables in pre-clinical and clinical medical research. *Cell Metabolism* 2016; 24:203–209. [PubMed: 27508869]
21. Rudnicki M, Abdifarkosh G, Rezvan O, Nwadozi E, Roudier E, Haas TL. Female mice have higher angiogenesis in perigonadal adipose tissue than males in response to high-fat diet. *Frontiers in Physiology* 2018; 9:1–15. [PubMed: 29377031]
22. Kjaer M, Kristjansdottir H, Andersen L, Heegaard AM, Agren M, Jorgensen LN. The effect of gender on early colonic anastomotic wound healing. *Int J Colorectal Dis* 2018; 33:1269–1276. [PubMed: 29850942]
23. Becker JB, Arnold AP, Berkley KJ, Blaustein JD, Eckel LA, Hampson E, Herman JP, Steiner M. Strategies and methods for research on sex differences in brain and behavior. *Endocrinology* 2005; 146:1650–1673. [PubMed: 15618360]
24. Prendergast BJ, Onishi KG, Zucker I. Female mice liberated for inclusion in neuroscience and biomedical research. *Neurosci Biobehav Rev.* 2014; 40:1–5. [PubMed: 24456941]
25. Becker JB, Prendergast BJ, Liang JW. Female rats are not more variable than male rats: a meta-analysis of neuroscience studies. *Biol Sex Differ.* 2016; 7:34–50. [PubMed: 27468347]
26. Mauvais-Jarvis F, Arnold AP, Reue K. A guide for the design of pre-clinical studies on sex differences in metabolism. *Cell Metabolism* 2017; 25:1216–1230. [PubMed: 28591630]
27. McClintock M. Estrous synchrony: modulation of ovarian cycle length by female pheromones. *Physiol Behav.* 1984; 32:701–705. [PubMed: 6541794]
28. Carmeliet P, Jain RK. Molecular mechanisms and clinical applications of angiogenesis. *Nature* 2011; 473:298–307. [PubMed: 21593862]
29. Potente M, Gerhardt H, Carmeliet P. Basic and therapeutic aspects of angiogenesis. *Cell* 2011; 146:873–887. [PubMed: 21925313]
30. DeBock K, Georgiadou M, Schoors S, et al. Role of PFKFB3-driven glycolysis in vessel sprouting. *Cell* 2013; 154:651–663. [PubMed: 23911327]
31. Lunt SY, Vander Heiden MG. Aerobic glycolysis: meeting the metabolic requirements of cell proliferation. *Annu Rev Cell Dev Biol.* 2011; 27:441–464. [PubMed: 21985671]
32. Yu P, Wilhelm K, Dubrac A, Tung JK, Alves TC, Fang JS, Simons M. FGF-dependent metabolic control of vascular development. *Nature* 2017; 545:224–232. [PubMed: 28467822]
33. Kalucka J, Bierhansl L, Vasconcelos Conchinha N, Missiaen R, Elia I, Bruning U, Cantelmo AR, Carmeliet P. Quiescent endothelial cells upregulate fatty acid β oxidation for vasculoprotection via redox homeostasis. *Cell Metabolism* 2018; 28:1–14. [PubMed: 29972795]
34. Doddaballapur A, Michalik KM, Manavski Y, Lucas T, Houtkooper RH, You X, Chen W, Potente M, Boon RA. Laminar shear stress inhibits endothelial cell metabolism via KLF2-mediated repression of PFKFB3. *Arterioscler Thromb Vasc Biol.* 2015; 35:137–145. [PubMed: 25359860]
35. Wilhelm K, Happel K, Eelen G, Schoors S, Oellerich MF, Lim R, Gerhardt H, Carmeliet P, Potente M. FOXO1 couples metabolic activity and growth state in the vascular endothelium. *Nature* 2016; 529:216–220. [PubMed: 26735015]
36. Dahlman-Wright K, Cavailles V, Fuqua SA, Jordan VC, Katzenellenbogen JA, Korach KS, Maggi A, Muramatsu M, Parker MG, Gustafsson JA. International union of pharmacology. LXIV. Estrogen receptors. *Pharmacol Rev.* 2006; 58:773–781. [PubMed: 17132854]
37. Lu NZ, Wardell SE, Burnstein KL, Defranco D, Fuller PJ, Giguere V, Wilson EM, McDonnell DP, Cidlowski JA. International union of pharmacology. LXV. The receptor superfamily:

- glucocorticoid, mineralocorticoid, progesterone, and androgen receptors. *Pharmacol Rev.* 2006; 58:782–797. [PubMed: 17132855]
38. Treps L, Conradi LC, Harjes U, Carmeliet P. Manipulating angiogenesis by targeting endothelial metabolism: hitting the engine rather than the driver—a new perspective? *Pharmacol Rev.* 2016; 68:8872–887.
 39. Xu Y, An X, Guo X, Habetsion TG, Wang Y, Xu X, Kandala S, Li Q, Li H, Zhang C. Endothelial PFKFB3 plays a critical role in angiogenesis. *Arterioscler Thromb Vasc Biol.* 2014; 34:1231–1239. [PubMed: 24700124]
 40. Meyer MR, Clegg DJ, Prossnitz ER, Barton M. Obesity, insulin resistance and diabetes: sex differences and role of oestrogen receptors. *Acta Physiol (Oxf)* 2011; 203:259–269. [PubMed: 21281456]
 41. Prossnitz ER, Arterburn JB. International union of basic and clinical pharmacology. SCVII. G protein coupled estrogen receptor and its pharmacologic modulators. *Pharmacol Rev.* 2015; 67:505–540. [PubMed: 26023144]
 42. Prossnitz ER, Hathaway HJ. What have we learned about GPER function in physiology and disease from knockout mice? *J Steroid Biochem Mol Biol.* 2015; 153:114–126. [PubMed: 26189910]
 43. Revankar CM, Cimino DF, Sklar LA, Arterburn JB, Prossnitz ER. A transmembrane intracellular estrogen receptor mediates rapid cell signaling. *Science* 2006; 307:1625–1630.
 44. Dennis MK, Field AS, Burai R, Ramesh C, Petrie WK, Bologna CG, Oprea TI, Yamaguchi Y, Hayashi S, Sklar LA, Hathaway HJ, Arterburn JB, Prossnitz ER. Identification of a GPER/GPR30 antagonist with improved estrogen receptor counterselectivity. *J Steroid Biochem Mol Biol.* 2011; 127:358–366. [PubMed: 21782022]
 45. Dennis MK, Burai R, Ramesh C, Petrie WK, Alcon SN, Nayak TK, Bologna CG, Leitao A, Bailois E, Deliu E, Dun NJ, Sklar LA, Hathaway HJ, Arterburn JB, Oprea TI, Prossnitz ER. In vivo effects of a GPR30 antagonist. *Nat Chem Biol.* 2009; 5:421–427. [PubMed: 19430488]
 46. Bologna CG, Revankar CM, Young SM, Edwards BS, Arterburn JB, Kiselyov AS, Parker MA, Tkachenko SE, Savchuck NP, Sklar LA, Oprea TI, Prossnitz ER. Virtual and biomolecular screening converge on a selective agonist for GPR30. *Nat Chem Biol.* 2006; 2:207–212. [PubMed: 16520733]
 47. Trenti A, Tedesco S, Boscaro C, Ferri N, Cignarella A, Trevisi L, Bolego C. The glycolytic enzyme PFKFB3 is involved in estrogen-mediated angiogenesis via GPER1. *J Pharmacol Exp Ther.* 2017; 361:398–407. [PubMed: 28348059]

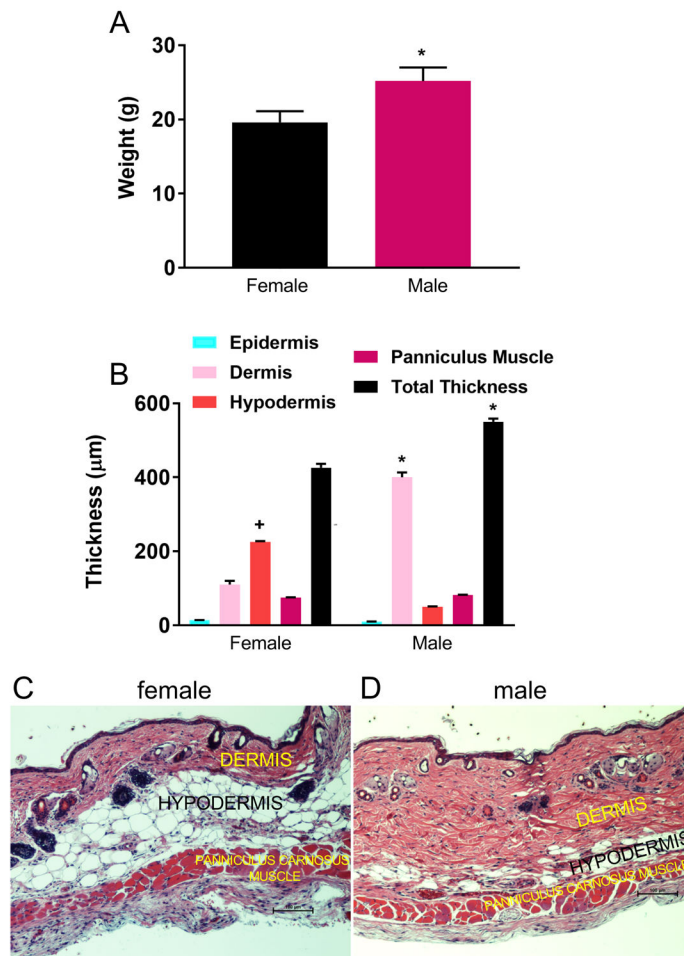


Figure 1. Body weights and control skin morphology.

A: Pre-operative weights of female and male mice (n=15 per sex, *p < 0.05 versus female mice). **B:** Nonoperative (control) skin thickness of female and male mice (n=5 per sex, +p < 0.05 versus male mice, *p < 0.05 versus female mice). **C:** Hematoxylin and eosin (H and E) stain of control female back skin and panniculus muscle illustrating reduced dermal and increased hypodermal proportions compared to male skin (black scale bar 100 µm). **D:** H and E stain of control male back skin and muscle. Note thick dermis and limited subcutaneous fat (hypodermis) (black scale bar 100 µm).

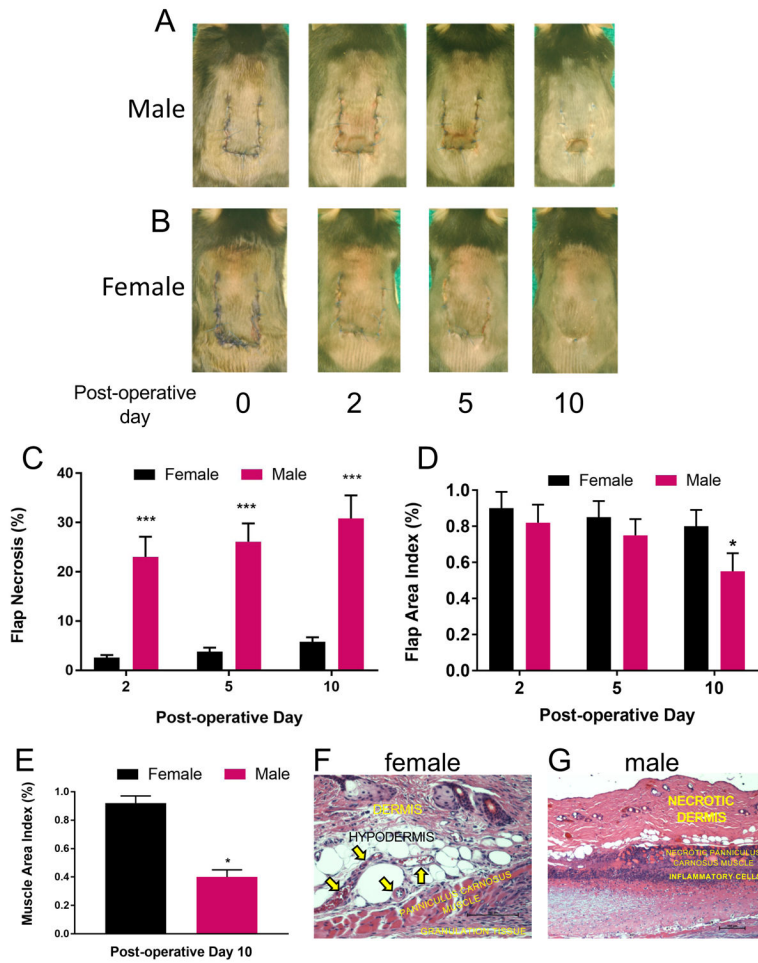


Figure 2. Flap viability and histopathology.

A: Documented by serial flap photography, note the early ischemia (post-operative day 2) and late necrosis (post-operative day 10) in a representative male flap. **B:** In contrast, note the lack of late (post-operative day 10) distal necrosis in a female flap. **C:** Planimetric determination of percentage of visible necrotic flap surface area at days 2, 5, and 10 (n=10 per sex, ***p < 0.001 versus female mice). **D:** Planimetric determination of the percentage of viable flap surface area at days 2, 5, and 10 (n=10 per sex, *p < 0.05 versus female flap at day 10). **E:** Quantitative determination of the histologic percentage of necrotic panniculus carnosus muscle at day 10 (n=10 per sex, *p < 0.05 versus female mice). **F:** H and E stain of day 10 distal female flap revealing viable dermis, hypodermis, and panniculus muscle with visible large vessels (arrows) in the subcutaneous fat and engraftment of muscle to underlying granulation tissue (black scale bar 100 μm). **G:** Day 10 distal male flap (H and E stain) revealing necrosis of epidermis, dermis, fat, and muscle with intense sub-flap inflammation and lack of engraftment to recipient site (black scale bar 100 μm).

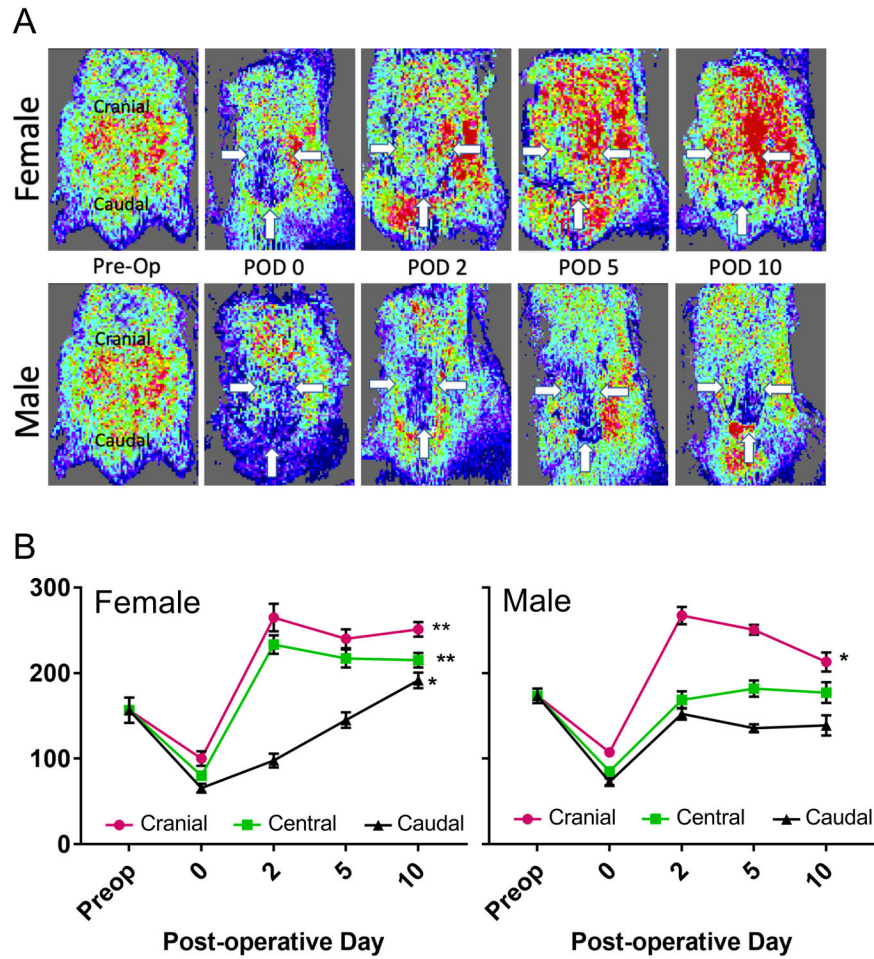


Figure 3. Perfusion imaging.

A: Representative serial laser speckle perfusion images of female and male flaps. Flap boundaries are outlined by arrows. Note the lack of distal flap reperfusion in the male mouse (blue intensity at caudal arrows). On post-operative day 10, male flap distal necrosis resulted in flap dehiscence and exposure of highly perfused panniculus muscle (red intensity near caudal arrow). Over the 10 day study interval, note the effective reperfusion of distal female flap (caudal arrows), and intense collateral perfusion (red intensity outside of lateral arrows).

B: Quantitative laser speckle perfusion of female flaps by ROI versus time (n=10, *p < 0.05, **p < 0.01 versus preop or control). Quantitative laser speckle perfusion of male flaps by ROI versus time (n=10, *p < 0.05 versus preop or control).

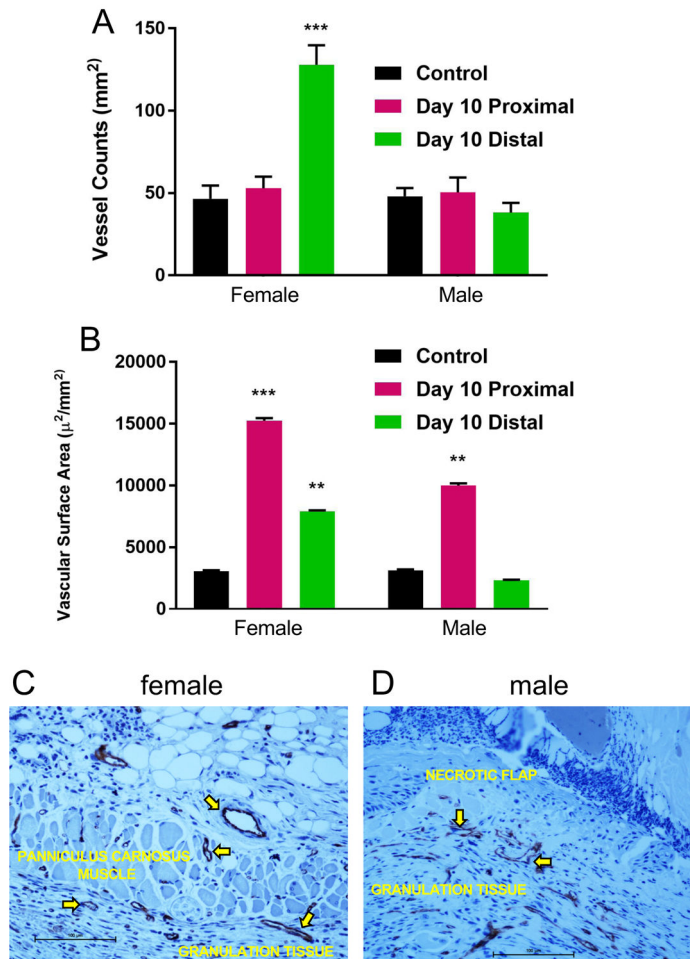


Figure 4. Microvascular anatomy and quantitation.

A: Quantitative vessel count of nonoperated mouse back myocutaneous tissue (control) and proximal and distal regions of flaps at day 10 (n=15 per sex, ***p < 0.001 versus same sex control). **B:** Quantitative vascular surface area estimates of control and proximal and distal regions of flaps at day 10 (n=15 per sex, **p < 0.01, ***p < 0.001 versus same sex control). **C:** Photomicrograph of female day 10 distal flap (CD-31 immunostaining, endothelium stains brown, black scale bar 100 µm). Note active angiogenesis in the recipient site granulation tissue (arrows) and marked neovascularization of the myocutaneous flap (arrows). **D:** CD-31 immunostained histologic section of male day 10 distal flap. Note active angiogenesis within the recipient granulation tissue (arrows) and lack of vascular ingrowth into the distal flap which is necrotic (black scale bar 100 µm).

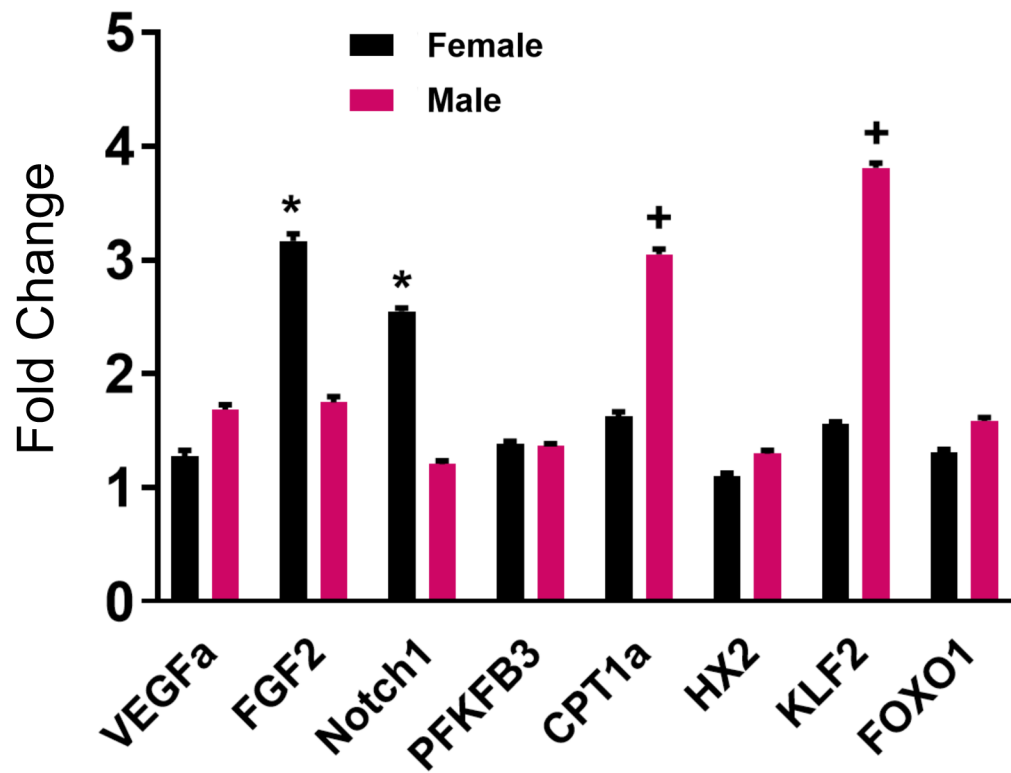


Figure 5. Local gene expression.

Day 10 flap gene expression (n=10 per sex, *p < 0.05 versus male mice, +p < 0.05 versus female mice).